Investigating the cyclic behaviour of clays using a kinematic hardening soil model

(Article begins on next page)

26 April 2024

Title:

Investigating the cyclic behaviour of clays using a kinematic hardening soil model

Author:

Gaetano Elia[1], Mohamed Rouainia[2]

[1] Lecturer in Geotechnical Engineering (Ph.D.), School of Civil Engineering & Geosciences, Newcastle University, NE1 7RU - Newcastle Upon Tyne, UK (corresponding author).

E-mail: gaetano.elia@ncl.ac.uk. Phone: +44 (0)191 2087934. Fax: +44 (0)191 2085322

[2] Senior Lecturer in Computational Geomechanics (Ph.D.), School of Civil Engineering & Geosciences, Newcastle University, NE1 7RU - Newcastle Upon Tyne, UK.

E-mail: mohamed.rouainia@ncl.ac.uk

Abstract

The stability of geotechnical structures under repeated loading depends to a large extent on the induced cyclic shearing stresses. The design of these structures usually requires engineers to employ advanced soil models in their analyses. While a number of such models do exist, their validation against cyclic laboratory tests is still very limited. In particular, the influence of the initial structure of the clay and its subsequent degradation under cyclic loading appears to be insufficiently investigated from both experimental and constitutive modelling standpoint.

The work outlined in this paper adds a new contribution to the theoretical understanding of cyclic response of clayey materials, presenting the extensive validation of an advanced kinematic hardening model against laboratory data on a number of natural and compacted clays found in literature. In order to analyse in detail the evolution of shear and hysteretic soil behaviour over a wide strain range, further modelling accounting for the effects of overconsolidation ratio and structure degradation is undertaken. The modelling results of shear stiffness degradation, hysteretic dissipation and pore pressure accumulation are presented and compared with experimental data. The results show that the enhanced kinematic hardening model gives very satisfactory predictions of clay response during cyclic loading.

1. Introduction

Saturated clayey deposits can be subjected to undrained cyclic loads by earthquakes, pile driving, traffic, explosions and storm waves. Under such repeated and irregular loading, clay structure deteriorates, pore water pressure changes and shear stiffness and strength degrade accordingly. Therefore, the behaviour of geotechnical structures and infrastructures interacting with clayey deposits is strongly influenced by the predictive capabilities of the constitutive model adopted for their design.

In particular, the characteristic features of the mechanical response of clays under cyclic loading, such as state dependency, early irreversibility, non-linearity, build-up of excess pore water pressures, decrease of nominal stiffness and related increase of hysteretic damping with cyclic shear strain, have been identified through extensive laboratory investigations on reconstituted samples by Sangrey et al. [1], Castro and Christian [2], Vucetic and Dobry [3], Yasuhara et al. [4], Matasović and Vucetic [5], Lee and Sheu [6] and Gu et al. [7], among others. More recently, there have been considerable advances in the experimental and constitutive modelling of natural soils to account for structure and its subsequent degradation under monotonic loading (e.g. Burland [8], Leroueil and Vaughan [9], Gens and Nova [10], Burland et al. [11], Cotecchia and Chandler [12], Callisto and Calabresi [13], Callisto and Rampello [14], Amorosi and Rampello [15]). Structure degradation under static loading has been shown to be critically important in reproducing the response of geotechnical systems interacting with clayey deposits, such as shallow foundations (e.g. Lagioia and Potts [16], Nova et al. [17]), earth embankments (e.g. Karstunen et al. [18], Panayides et al. [19]) and tunnels (e.g. Gonzáles et al. [20]). In contrast, only few contributions can be found in literature where the damage to structure caused by cyclic loading is accounted for in the analysis (e.g. Elia and Rouainia [21]). It is well-known that natural clays exhibit higher small-strain stiffness (G_0) than the corresponding reconstituted materials (Rampello et al. [22, 23], Viggiani and Atkinson [24], Rampello and Viggiani [25], Cafaro and Cotecchia [26]). However, it appears that little research has been directed towards

understanding the evolution of microstructure (destructuration) during cyclic loading and its effect on the normalised shear modulus (G/G_0) degradation curve, excess pore water pressure (Δu) and damping (D) curves with cyclic shear strain (γ). Only few laboratory data presenting a direct and consistent comparison between the cyclic/dynamic behaviour of natural and reconstituted samples of the same material are available in the literature. d'Onofrio *et al.* [27, 28] reported the results of an extensive testing programme on two natural Italian stiff clays using a resonant column/torsional shear device. In particular, the normalised shear modulus reduction curves obtained by testing a reconstituted (4BSR04) and a natural sample (1BSI04) of Bisaccia clay at the same mean confining pressure of 50 kPa are shown in Figure 1a. It can be observed that the normalised shear stiffness of the natural sample degrades faster than the corresponding reconstituted material and the authors highlighted that the linear threshold strain of the natural specimens is always smaller than that of the reconstituted samples in all their experiments. Rampello and Silvestri [29] also presented experimental G/G_0 degradation curves for natural and reconstituted samples of overconsolidated Vallericca clay obtained during resonant column (RC) and torsional shear (TS) tests (see Figure 1b). Allman and Atkinson [30] and Atkinson *et al.* [31] reported the secant shear modulus (G_{sec}) normalised with respect to the initial mean effective stress (p_0) for intact and reconstituted samples of Bothkennar clay obtained from undrained triaxial (TRX) tests (Figure 1c). These experimental results showed that natural clays, although characterised by initial higher small-strain stiffness, exhibit smaller normalised shear stiffness than reconstituted soils due to damage to structure caused by the increased loading throughout the test.

In the simpler constitutive relations, the shear modulus degradation is indirectly obtained from a hyperbolic function that describes the backbone curve (e.g. Ramberg and Osgood [32], Iwan [33], Duncan and Chang [34]). Unloading-reloading behaviour is modelled by sets of rules, such as those proposed by Masing [35] or Pyke [36], which control the shape of hysteresis loops and, therefore, the damping of the soil. One of the limitations of these basic models is that they tend

4

1 to overestimate the damping in the medium to large strain range and to under-predict it for small

2 shear strains (Puzrin and Shiran [37]). Attempts have been made in recent years to improve the

3 predictive capabilities of these simple hyperbolic models, trying to fit both the experimental

4 normalised shear modulus and the damping ratio curve over the entire range of cyclic shear

5 strain amplitudes (e.g. Darendeli [38], Phillips and Hashash [39]). Nevertheless, the stress-strain

6 response predicted by these enhanced models is still decoupled from the generation of excess

7 pore pressures, as the formulation is developed in terms of total stress. Alternatively, more

8 advanced constitutive laws have been developed to capture the mechanical behaviour of

9 cohesive materials within the framework of the work-hardening elasto-plasticity theory (e.g.

10 Mroz *et al*. [40], Prevost [41] and Dafalias and Herrmann [42]). The presence of soil structure

11 and its subsequent degradation under increased loading has been recently included into a number

12 of elasto-plastic constitutive models, such as those proposed by Asaoka *et al.* [43], Rouainia and

13 Muir Wood [44], Kavvadas and Amorosi [45], Baudet and Stallebrass [46] and Seidalinov and

14 Taiebat [47]. These effective-stress-based models are able to describe the response of natural

15 clays under both monotonic and cyclic loading conditions, accounting for the accumulation of

16 plastic strains and shear induced excess pore water pressures with increasing number of cycles.

17 Nevertheless, the essential aspect of the influence of soil structure on small-strain stiffness has

18 not been incorporated in these models.

19 The aim of the paper is to investigate the performance of one of these non-linear constitutive

20 models during cyclic shear simulations representing advanced dynamic laboratory tests on clays

21 (such as RC and TS tests). The first part of the work introduces a modification of the well-known

22 expression proposed by Viggiani and Atkinson [24] for the variation of G_0 with current state,

23 which allows to independently account for the influence of mean effective stress,

24 overconsolidation ratio and soil structure on shear stiffness. The new elasticity formulation has

25 been implemented into an existing multi-surface kinematic hardening model, the Rouainia and

26 Muir Wood (*RMW*) model [44], to enhance its predictive capabilities under static and cyclic

1 loading conditions. The influence of model parameters and state variables on the *RMW*

2 predictions of *G-γ*, *D-γ* and *Δu-γ* curves has been then investigated through an extensive

3 parametric study. Finally, the modified constitutive model has been validated using experimental

4 data on natural, reconstituted and compacted clays found in literature.

5

6 **2. Soil constitutive model**

7 The constitutive model adopted in this work has been formulated for natural clays by Rouainia

8 and Muir Wood [44] within the framework of kinematic hardening with elements of bounding

9 surface plasticity. This model converges to the Modified Cam-Clay model for remoulded

10 structureless soils. It is characterised by three surfaces in the stress space (see Appendix I). The

11 reference surface (f_r) controls the state of the soil in its reconstituted, unstructured form and

12 describes the intrinsic behaviour of the clay (Burland [8]). The structure surface (*F*) controls the

13 process of destructuration which can be accompanied by significant strain-softening effects. The

14 bubble (f_b) encloses the elastic domain of the soil and moves within the structure surface

15 following a kinematic hardening rule. The decrease of stiffness with strain is controlled by an

16 interpolation function which ensures a smooth movement of the elastic domain towards the

17 structure surface during loading.

18 The Rouainia and Muir Wood model has been implemented in the single element driver *SM2D*

19 (Chan [48]) with an explicit stress integration algorithm adopting a constant strain sub-stepping

20 scheme. Appendix I reports its governing equations. The model has been successfully employed

21 to simulate both static (Panayides *et al.* [19], Gonzáles *et al.* [20]) and dynamic geotechnical

22 problems (Elia and Rouainia [21, 49]). Nevertheless, the performance of *RMW* has never been

23 extensively validated against cyclic laboratory data before.

24 In previous versions of the model a classical hypoelastic formulation, accounting for a linear

25 dependence of both bulk and shear moduli on mean effective pressure, was adopted. In this

26 work, a different elasticity formulation has been implemented to include the dependency of the

1   shear modulus on the overconsolidation ratio and soil structure. To this aim, the well-known

2   equation proposed by Viggiani and Atkinson [24] for the small-strain shear modulus (G_0) has

3   been modified as follows:

4

5    $$\frac{G_0}{p_r} = A \left(\frac{p}{p_r} \right)^n R_0{}^m r^l$$ (1)

6

7   where A, m and n are dimensionless stiffness parameters, p_r is a reference pressure (equal to 1

8   kPa), p is the mean effective stress (with the prime dropped for simplicity), r is the *RMW* model

9   parameter accounting for soil structure due to bonding (see Appendix I) and $R_0 = 2r_0 p_c / p_0$ is the

10   isotropic overconsolidation ratio. For $r = 1.0$ (i.e. no structure), Equation (1) reduces to the

11   original expression of Viggiani and Atkinson [24]. With respect to the original formulation,

12   Equation (1) introduces only one additional parameter, l, which controls the contribution of

13   structure to the model prediction of shear modulus. The new expression resembles the one

14   originally proposed by Cafaro and Cotecchia [26] for stiff clays and recently suggested by

15   Trhlíková *et al*. [50] for the small-strain behaviour of cemented soils.

16

17   **3. Parametric investigation**

18   In using advanced constitutive models for the design of geotechnical structures subjected to

19   cyclic/dynamic loads, special emphasis has to be given to the calibration procedure of their

20   numerous parameters and the initialization of their state variables (i.e. initial stress state and

21   hardening parameters) based on laboratory and in-situ data.

22   The distinct and combined effects of the overconsolidation ratio and soil structure, together with

23   model parameter selection on the *RMW* predictions of cyclic response of clays have been

24   systematically investigated in this part of the study. For all the simulations presented in this

25   section, a typical set of model parameters (Set 1) has been assumed for the parametric analysis

1   (see Table 1). The stiffness parameters A, m and n, equal to 770, 0.23 and 0.82, respectively,

2   have been chosen to be representative of a clayey soil with a plasticity index of 35%, using the

3   correlation proposed by Viggiani and Atkinson [24]. A critical state ratio of 1.2, corresponding

4   to a friction angle of 30° during triaxial compression, and a constant Poisson's ratio equal to 0.25

5   have been adopted. A small size of the bubble surface (represented by a ratio of $R = 0.1$) has

6   been assumed to account for early development of plastic strains during loading. In addition, a

7   default value of 0.5 has been used for the parameter A^*, thus assuming an equal proportion of

8   distorsional and volumetric destructuration. The parameter k controlling the rate of loss of

9   structure with damage strain has been set equal to 1.0. A series of single element simulations of

10   strain-controlled undrained cyclic simple shear (CSS) tests have been carried out by imposing

11   different shear strain amplitudes and assessing the model response for each strain value after a

12   number of cycles sufficient to reach a steady-state condition. In particular, the secant shear

13   modulus, the damping ratio and the excess pore pressures predicted during undrained loading

14   have been determined after 500 strain cycles, as suggested by Elia [51] and Elia *et al.* [52]. This

15   approach is slightly different from the one originally proposed by Seed *et al.* [53] and recently

16   adopted by Seidalinov and Taiebat [47], which consists of the evaluation of the shear modulus

17   and damping ratio at the fifth cycle of the stress-strain loop of a cyclic shear test. Five load

18   cycles are, in fact, considered not to be sufficient to reach a steady-state condition and to

19   represent an appropriate simplification of real RC and TS tests, where thousands of loading

20   cycles are applied to the soil sample. Moreover, the effect of the number of cycles (N) on the

21   material cyclic degradation and pore water pressure generation has been widely observed during

22   laboratory investigations on clays (e.g. Vucetic [54], Vucetic and Dobry [3]) and should be

23   accounted for in the constitutive modelling simulations.

24

25   *3.1 Effect of overconsolidation ratio*

26   Initially, the performance of *RMW* has been evaluated assuming a fixed initial value of the state

1   variable p_c, which controls the size of the reference surface, and changing the mean effective

2   confining pressure in order to simulate CSS tests at different overconsolidation ratios (R_0 equal

3   to 1.0, 1.5, 2.0, 3.0 and 4.0). In this set of simulations, the effect of the initial structure has not

4   been accounted for ($r_0 = 1.0$).

5   Figure 2a presents the results of CSS test simulations performed at different shear strain levels in

6   terms of normalised shear modulus reduction curves and corresponding variations of damping

7   ratio with γ. The new elastic formulation of the model (i.e. Equation (1)) is now able to capture

8   the increase of G_0 with overconsolidation. Nevertheless, the normalised G/G_0-γ curves reported

9   in Figure 2a are not independent of R_0, as clay samples characterised by higher overconsolidation

10   ratios show a larger linear cyclic response at small strains and their stiffness degrades less than

11   normally consolidated soils at large strains. The overconsolidation has instead a small effect on

12   the calculated D-γ curves, consistently with the laboratory evidences (e.g. Vucetic and Dobry

13   [3]). Figure 2b shows the normalised excess pore pressure curves ($\Delta u/p_0$) calculated with *RMW*

14   for different R_0 values: in normally consolidated and slightly overconsolidated cases (i.e. R_0

15   equal to 1.0 and 1.5) positive excess pore pressures are predicted, whereas for higher

16   overconsolidation ratios (3.0 and 4.0) negative pore water pressures are accumulated during the

17   cycles.

18   In the model, the amount of Δu generated during a cyclic test is directly controlled by the

19   distance between the initial mean effective stress p_0 and the centre of the reference surface p_c,

20   i.e.:

21

22   $$\frac{\Delta u}{p_0} = \frac{p_0 - p_c}{p_0} \qquad (2)$$

23

24   as the stress path starts from p_0 and tends to reach a steady-state condition at critical state. This is

25   shown schematically in Figure 3a, where the stress paths of two strain-controlled undrained TRX

1   simulations, one starting from a slightly overconsolidated state and one from a highly

2   overconsolidated state, are reported. The arrows in the figure represent the stress path directions.

3   When R_0 is 1.0, the distance between the initial mean effective stress and the centre of the

4   reference surface is equal to the size of the reference surface p_c, while p_0 is twice p_c and therefore

5   the normalised excess pore pressure is 0.5 according to Equation (2). For R_0 equal to 2.0, the

6   model predicts a value of Δu equal to zero, being $p_0 = p_c$. In this case, the stress path starts from

7   the centre of the reference surface and remains vertical during the cycles with no accumulation

8   of pore pressures. When R_0 is 4.0, $\Delta u/p_0$ is equal to -1.0, being p_0 half of p_c. Figure 2b also

9   indicates that for small shear strains the excess pore pressures are equal to zero as the imposed

10   shear strain level is not sufficiently high to produce plastic strains. This corresponds to a null

11   damping ratio in Figure 2a. Moreover, for $\gamma \geq 0.05\%$ the calculated excess pore pressures during

12   different CSS tests performed at the same overconsolidation ratio remain constant and equal to

13   the value predicted by Equation (2), no matter what level of cyclic shear strains is considered.

14   This happens because the number of cycles selected for the CSS simulations (i.e. 500) is

15   sufficient to attain a steady-state condition during each test.

16

17   *3.2 Effect of structure and its degradation*

18   In this part of the work, a set of CSS tests have been simulated with the modified *RMW* model by

19   imposing the same initial value of the state variable p_c and considering four different degrees of

20   initial structure (i.e. $r_0 = 1.0, 1.5, 2.0$ and 3.0). The soil has been assumed normally consolidated

21   (i.e. $R_0 = 1.0$) in order to clearly separate the effects of overconsolidation from those due to

22   structure degradation. In addition, the parameter l has been assumed equal to 0.25, while its

23   effect is presented later in this section.

24   Figure 4a shows the normalised shear modulus reduction curves for the different assumed r_0

25   values: samples with higher initial structure tend to have a less linear cyclic response at small

1   strains and their stiffness degrades more than structureless soils at larger strains. The G/G_0

2   curves for structured soils are consistently shifted to the left in comparison with the one of the

3   unstructured material due to structure degradation induced by the cyclic loading in the medium

4   to large strain range. The initial structure, on the contrary, seems to have a negligible effect on

5   the predicted behaviour in terms of hysteretic dissipation (Figure 4a). Moreover, the results

6   reported in Figure 4b, in terms of variation of $\Delta u/p_0$ with γ, indicate that positive excess pore

7   pressures are generated during the cycles in all cases, as the soil is normally consolidated. Their

8   normalised large-strain value is controlled, according to Equation (2), by the size of the reference

9   structure p_c, which is now different in the four cases. For higher r_0 values, the shear modulus

10   starts to decay at smaller shear strain levels and non-zero damping ratios and excess pore

11   pressures are predicted accordingly. While 500 cycles have been proved to be sufficient to reach

12   a steady-state condition during the CSS simulations with different R_0 and no structure (Figure

13   2b), Figure 4b indicates that this number of loading cycles appears to be insufficient to induce a

14   full destructuration of the samples, especially at small-strain levels.

15   The effect of the parameter l introduced in Equation (1) on the cyclic response predicted by the

16   new version of *RMW* model has also been explored. The normalised $G\text{-}\gamma$ curves obtained during

17   a set of CSS test simulations on normally consolidated structured samples (r_0 equal to 1.5) are

18   reported in Figure 5a, for values of l ranging from 0.25 to 1.0. The behaviour predicted by

19   changing l is qualitatively similar to what described in Figure 4a, where r_0 is varied.

20   Nevertheless, the parameter l influences the initial shear stiffness while r_0 controls also the

21   degree of soil structure and the evolution of the destructuration process. Therefore, a narrower

22   variation in the $G/G_0\text{-}\gamma$ curves can be observed in Figure 5a with respect to Figure 4a, as the

23   degree of initial structure is fixed in this case (i.e. $r_0 = 1.5$). The $D\text{-}\gamma$ curves reported in the same

24   Figure 5a confirm the negligible effect of soil structure on the hysteretic dissipation predicted by

25   the model. The results shown in Figure 5b in terms of normalised excess pore water pressures

11

1 highlight the minor influence of l on the accumulation of pore water pressures during large-strain

2 cycles, consistently with what observed in terms of damping.

3 Finally, Figure 6a shows the normalised G-γ curves obtained during CSS test simulations on

4 normally consolidated structured samples ($r_0 = 2.0$) for different values of the parameter k

5 ranging between 0 and 2.0 (where k controls the rate of structure degradation with damage

6 strain). The parameter A^* has been assumed equal to 0.5, as in all previous simulations. With

7 respect to the default case of $k = 1.0$ (see Table 1), the simulations performed assuming k equal

8 to 2.0 exhibit a smaller normalised shear stiffness. In contrast, the slower rates of loss of

9 structure (i.e. $k = 0.5$ and 0.1) produce consistently stiffer shear modulus degradation curves, for

10 which the upper limit is represented by the curve obtained with $k = 0$ (no destructuration). In all

11 cases, the destructuration rate plays only a role when large shear cycles are imposed, while the

12 G-γ curves completely overlap for $\gamma < 0.01\%$. Moreover, the effect of k on the damping curves is

13 also negligible, as reported in Figure 6a. The normalised excess pore water pressure curves,

14 shown in Figure 6b, confirm that the full destructuration only occurs for large imposed shear

15 strains, while partial loss of structure is observed in the medium to small strain range. When no

16 destructuration is allowed ($k = 0$), the normalised Δu-γ curve resembles the one of a normally

17 consolidated unstructured soil (see Figure 2).

18 In general, Figures 4, 5 and 6 show that the initial structure and its subsequent degradation have

19 an opposite effect on the predicted soil behaviour during cyclic loading with respect to

20 overconsolidation (see Figure 2), thus indicating that these are two distinct aspects of the

21 mechanical behaviour of natural clays. Note that the model is able to capture the softer shear

22 modulus degradation of natural clays when compared with reconstituted clays, which can be

23 seen experimentally in Figure 1.

24

25 *3.3 Combined effect of overconsolidation and structure*

1   To investigate the simultaneous influence of overconsolidation and structure, CSS simulations

2   has been performed on structured samples ($r_0 = 3.0$) assuming different initial conditions in

3   terms of R_0. As in the previous simulations, the parameter l has been set equal to 0.25.

4   Figure 7a reports the modulus degradation and damping curves predicted by *RMW* in this case:

5   as previously observed (Section 3.1), higher overconsolidation ratios induce larger linear cyclic

6   response at small strains, followed by steeper stiffness degradation at larger strains.

7   Nevertheless, the presence of structure considerably affects the build-up of excess pore

8   pressures, as shown in Figure 7b. For normally and slightly overconsolidated samples (i.e. R_0

9   equal to 1.0 and 1.5), the cumulated pore water pressures are always positive, indicating a

10   contracting behaviour during the cycles. This is observed also when R_0 is equal to 2.0, as the

11   structure degradation induced by the cycles implies that the stress state always lies on the "wet"

12   side of critical state (as defined by Roscoe and Burland [55]) during the test. In contrast, when

13   the overconsolidation is higher than 2.0 the initial stress state of the samples is located on the

14   "dry" side of critical, thus inducing an initial accumulation of negative pore pressures. Then, due

15   to the concurrent contraction of the structure surface, the overconsolidation ratio reduces leading

16   to the generation of positive excess pore water pressures in the final part of the cyclic

17   simulations. This fundamental mechanical behaviour of natural clays under cyclic loading is also

18   illustrated in Figure 3b, where the stress paths of strain-controlled undrained triaxial simulations

19   on slightly and highly overconsolidated structured samples are shown in the $p : q$ plane. In the

20   slightly overconsolidated case, the stress path moves from right to left until all structure has been

21   lost. In contrast, for the case of highly overconsolidated sample, the stress path initially moves to

22   the right and then travels back due to the contraction of the structure surface. Arrows are shown

23   in the figure to depict the contraction of the structure surface together with the stress path

24   directions.

25

26   *3.4 Effect of stiffness interpolation parameters*

1   The *RMW* predictions discussed in the previous sections of this paper have shown the capability

2   of the model to capture some crucial features of the cyclic behaviour of clays, highlighting the

3   importance of the material overconsolidation and structure. Nevertheless, it should be noted that

4   the damping predicted by the model for small strains (i.e. $\gamma \leq 0.01\%$) is equal to zero, whereas

5   the experimental data (e.g. Vucetic and Dobry [3]) typically indicate an initial damping ratio D_0

6   of about 2%. *RMW* can only simulate hysteretic dissipation caused by plastic strains, which are

7   practically zero for small values of imposed γ as the associated stress paths lie inside the bubble

8   surface. Smaller bubble sizes (controlled by the parameter R) could allow the prediction of an

9   earlier development of plastic strains and related damping. At the same time, it has been argued

10   that the D_0 values measured in RC experiments can be attributed to material viscous effects

11   and/or the inertia of the resonant column apparatus itself (Meng and Rix [56]), which cannot be

12   accounted for in *RMW*. Additionally, the model tends to over-predict the damping ratio at large

13   strains ($\gamma \geq 0.5\%$) with respect to laboratory data (e.g. Vucetic and Dobry [3]). The shape of the

14   hysteretic loops is controlled by the elasto-plastic stiffness during loading-unloading cycles and,

15   therefore, by the stiffness interpolation parameters B and ψ used in the plastic modulus

16   interpolation function (Equation (I8) in the Appendix). To investigate their effect on the

17   hysteretic damping predictions of the modified version of *RMW*, the parameter B has been varied

18   between 0.1 and 2.5 for a fixed ψ equal to 1.5 and ψ has been changed between 0.1 and 2.5 for a

19   fixed $B = 1.0$, while the values reported in Table 1 have been adopted for all the other model

20   parameters. No overconsolidation and initial structure have been considered (i.e. $R_0 = r_0 = 1.0$).

21   Figures 8a and 8b show the corresponding G/G_0-γ and D-γ curves together with the range of

22   experimental data by Vucetic and Dobry [3], reported with a shaded area. Compared to the case

23   where $B = 1.0$ and $\psi = 1.5$, a significant reduction in the damping ratio over-prediction at large

24   strains can be obtained if smaller values of B (e.g. 0.1) and larger values of ψ (e.g. 2.5) are

25   employed, as the predicted response during unloading-reloading cycles is softer and,

1   consequently, the area of the loops is smaller. On the contrary, larger B and smaller ψ values

2   make the plastic modulus larger, thus leading to a stiffer response at large strains and wider

3   hysteretic loops. Although a careful calibration of the stiffness interpolation parameters can

4   improve the prediction by the enhanced *RMW* model of plastic dissipation, the damping curves

5   still plot higher than the experimental data for $\gamma > 0.5\%$. Slight improvements would have been

6   obtained by employing the structure degradation feature of the model, whereas the parametric

7   investigation suggests that a modification of the plastic modulus interpolation function could

8   lead to better predictions of hysteretic damping in the large-strain range.

9

10   **4. Model validation against laboratory data**

11   The modified *RMW* model has been validated against undrained cyclic tests performed on three

12   different clays: a compacted clay from Thailand (Soralump and Prasomsri [57]), reconstituted

13   samples of the VNP (Venezuelan North of Paria) clay (Vucetic [54]), and the natural Cloverdale

14   clay (Zergoun and Vaid [58]). The corresponding model parameters and initial state variables are

15   given by Set 2, Set 3 and Set 4 in Tables 2 and 3, respectively. In all these simulations, the

16   stiffness parameters A, m and n in Equation (1) have been selected as function of the plasticity

17   index using the correlation proposed by Viggiani and Atkinson [24], while a value of 0.25 has

18   been used for the parameter l.

19

20   *4.1 Compacted clay*

21   Soralump and Prasomsri [57] conducted a series of cyclic hollow cylinder torsional tests on

22   compacted clay specimens collected from different types of dams in Thailand. The samples were

23   prepared by wet hand-tamping compaction, fully saturated and isotropically consolidated up to

24   the maximum effective confining pressure. The overconsolidated specimens were subsequently

25   unloaded to the desired effective confining pressure to achieve the required overconsolidation

26   ratio. In the cyclic shearing phase of the tests, the samples were torsionally sheared under

1   undrained condition in six to eight multi-stages, imposing 10 cycles in each stage. The strain-

2   controlled shearing was conducted with a frequency of 2 Hz and the applied shear strain

3   amplitude (γ_c) was varied in the range of approximately 0.005 to 1.5% (Figure 9a). In general,

4   the results of this study revealed that overconsolidation significantly affects the stiffness

5   degradation and cyclic pore water pressure in compacted clay specimens. The ones with higher

6   overconsolidation ratios exhibited less degradation and larger initial accumulation of negative

7   pore pressures before a final build-up of positive pressures. In particular, the test performed

8   under an effective confining stress (σ'_c) of 100 kPa on a sample with an overconsolidation of 4,

9   an optimum moisture content of about 19%, a liquid limit of 35% and a plasticity index of 17%

10   is considered here. The observed changes in normalised cyclic shear stress (τ_c^*) and normalised

11   pore water pressure (r_u) are plotted in Figures 9b and 9c, respectively.

12   In the *RMW* calibration process, a critical state ratio of 1.4, corresponding to a friction angle of

13   34° during triaxial compression, has been adopted, while the ratio of sizes of bubble and

14   reference surface has been set equal to 0.07. As in the parametric investigation presented in

15   Section 3, an equal proportion of distorsional and volumetric destructuration has been assumed

16   (i.e. $A^* = 0.5$) but a lower rate of loss of structure with damage strain ($k = 0.5$) has been used.

17   Calibration of the stiffness interpolation parameters B and ψ has been performed based on the

18   stress-strain loops of the undrained cyclic shear stress tests. The corresponding model

19   predictions, adopting the parameters and state variables given by Set 2 in Tables 2 and 3, are in

20   good agreement with the experimental data, as indicated by Figures 9d, 9e and 9f. Consistently

21   with the experiments, the normalised cyclic shear stress decreases with the number of cycles,

22   especially in the last five stages of the test, with a larger reduction as the magnitude of shear

23   strains increases (Figure 9e). The measured and predicted stress-strain loops are reported in

24   Figures 10a and 10b, respectively. While the general trend is correctly captured by the *RMW*

25   model, the shape of the loops simulated with the model is different from the observed one. This

1   discrepancy can be attributed to the nature of the tested material, which presumably contained a

2   high percentage of non-fine particles in order to be compacted to the optimum moisture content

3   and, therefore, showed a cyclic mobility response at large strains typical of granular materials. It

4   can also be guessed that some sort of structure has been generated by the compaction of the

5   specimens (and therefore $r_0 = 3.0$ has been used in the simulations), thus leading to the initial

6   generation of negative pore water pressures then followed by a final build-up of positive excess

7   pore pressures (Figure 9c). As discussed in the previous Section 3.3, *RMW* is able to capture this

8   observed behaviour in terms of r_u when the effects of overconsolidation and structure are

9   concurrently taken into account (Figure 9f). Nevertheless, the amount of negative excess pore

10   pressures accumulated during the first four stages of the numerical simulations is considerably

11   higher than the one measured during the experiment. Again, this may be due to the specific

12   nature of the tested compacted clays, for which Soralump and Prasomsri [57] measured cyclic

13   pore water pressures consistently lower than those previously obtained using other types of clays

14   tested in other types of devices at corresponding cyclic shear stain amplitudes.

15   Additional CSS simulations have been performed following the procedure explained in Section 3

16   in which the same model parameters and initial state variables given in Tables 2 and 3 have been

17   used. The results of these simulations are reported in Figures 7a and 7b in terms of G/G_0-γ, D-γ

18   and $\Delta u/p_0$-γ curves. It can been seen that the curves for the compacted clay show a rapid

19   degradation of shear stiffness and development of excess pore water pressures compared to those

20   predicted in the parametric analysis using the same initial degree of structure ($r_0 = 3.0$) and

21   overconsolidation ratio ($R_0 = 4.0$). This can be attributed to the differences in the remaining

22   model parameters, in particular the stiffness interpolation values. Consistently with the results

23   discussed in Section 3.4, the large-strain damping ratio is lower compared the one obtained in the

24   parametric study.

25

26   *4.2 Venezuelan North of Paria (VNP) clay*

1   A series of experimental data by Vucetic [54] on reconstituted samples of the VNP clay has been

2   used here for the calibration and validation of the *RMW* model. The VNP clay is a blue-grey stiff

3   to medium plasticity clay with traces of organic content and some silt. The water content after

4   consolidation ranged from 41 to 49%, the liquid limit from 71 to 93% and the plasticity index

5   was equal to $45 \pm 6\%$. The laboratory data included oedometer tests, undrained monotonic and

6   undrained cyclic shear tests. In particular, two undrained cyclic shear tests, one performed on a

7   normally consolidated (NC) and the other on an overconsolidated (OC) sample, have been

8   considered. The stress-strain loops for the two laboratory tests are reported in Figures 11a and

9   11b, respectively, in terms of normalised cyclic shear stress (τ_h^*) versus imposed shear strain (γ).

10   The one-dimensional consolidation tests have been used to calibrate the parameters λ^* and κ^*

11   of the model, while the critical state stress ratio M_θ has been obtained from undrained

12   monotonic shear tests. Calibration of the stiffness interpolation parameters B and ψ has been

13   performed based on the stress-strain loops of the undrained cyclic shear stress tests. Although the

14   VNP specimens have been reconstituted in the laboratory before testing, a small amount of initial

15   structure has been introduced in the numerical simulations ($r_0 = 1.3$) together with a high rate of

16   destructuration ($k = 2.0$) in order to capture the stiffness degradation during cycles shown in

17   Figures 11a and 11b. The model parameters and state variables adopted in this case are given by

18   Set 3 in Tables 2 and 3, respectively. The corresponding *RMW* predictions, presented in Figures

19   11c and 11d, are in good agreement with the experimental results, showing a similar decrease of

20   the cyclic secant shear modulus with the number of cycles.

21   The results of CSS test simulations performed using the set of parameters and state variables of

22   the VNP clay (Set 3) are shown in Figures 4 and 7 for the normally consolidated and

23   overconsolidated states, respectively. The comparison with the parametric analysis presented in

24   Section 3.2 indicates that a softer response of the normally consolidated VNP clay accompanied

25   with smaller hysteretic loops at large strains is predicted (Figure 4a). However, the development

1 of excess pore water pressure is in good agreement with the results obtained in the parametric

2 analysis (Figure 4b). The same conclusions can be drawn for the overconsolidated VNP clay in

3 terms of G/G_0-γ and D-γ curves (Figure 7a). The normalised Δu-γ curve of the VNP clay,

4 depicted in Figure 7b, resembles the one obtained for an overconsolidated and unstructured soil

5 (see Figure 2), since the VNP clay initial degree of structure is very small.

6

7 *4.3 Cloverdale clay*

8 Finally, the experimental data by Zergoun and Vaid [58] on undisturbed structured samples of

9 Cloverdale clay have been used in this section for the validation of the modified *RMW* model.

10 This is a soft grey natural clay that has been deposited in a marine environment and is

11 characterised by a natural water content equal to 50%, a liquid limit of 50% and a plasticity

12 index of 24%. Its sensitivity (i.e. initial structure) it is due to surface infiltration following an

13 uplift above the sea level. Undrained cyclic triaxial tests performed at different imposed cyclic

14 stress ratio amplitude (τ_c/c_u), ranging between 0.62 and 0.79, on hydrostatically normally

15 consolidated samples under an effective stress of 200 kPa have been considered here. Figure 12

16 presents the development with the number of cycles (N) of the axial strain (ε_a) at peaks of cyclic

17 stress measured during the experiments (reported with symbols). Dealing with structured

18 specimens of a natural clay has suggested to adopt a relatively high initial degree of structure (r_0

19 = 3.0). A slightly higher proportion of distorsional destructuration ($A^* = 0.6$) and a low rate of

20 loss of structure with damage strain ($k = 0.1$) have been assumed in this case. The other model

21 parameters have been obtained from Seidalinov and Taiebat [47], who have calibrated a

22 bounding surface model against the same laboratory tests on Cloverdale clay [58]. The resulting

23 *RMW* parameters and state variables are given by Set 4 in Tables 2 and 3 and the corresponding

24 undrained cyclic triaxial simulations are shown in Figure 12 with dashed lines. The predicted

25 accumulation of peak ε_a for τ_c/c_u equal to 0.75, 0.69 and 0.62 are closely matching the

experimental results. For τ_c/c_u equal to 0.79, instead, the model predicts a stiffer behaviour both during compression and extension. Although the overall trend of response is captured, this validation process confirms the necessity to modify the plastic modulus interpolation function of *RMW* to better capture the evolution of stress-strain loops observed in the experiments for large imposed stress ratios.

The calibrated material parameters and state variables have been assigned to the Cloverdale clay in the CSS test simulations. The comparison between the simulated and parametric study also shows good agreement (Figure 4) for the initial degree of structure $r_0 = 3.0$ and an overconsolidation ratio $R_0 = 1.0$.

5. Conclusion

The enhanced version of a multi-surface kinematic hardening model implementing a new elastic formulation for the variation of G with mean effective stress, overconsolidation ratio and soil structure has been presented in the paper. The model prediction of shear stiffness degradation, hysteretic dissipation and pore pressure accumulation has been parametrically investigated by changing the model parameters and state variables. This has allowed to study the effects of overconsolidation and structure degradation on the evolution of shear and hysteretic behaviour predicted using the advanced soil model. The effect of initial anisotropy on clay cyclic response has not been considered in the present paper, but this could be investigated in future work. The numerical results presented in the paper have shown that:

i. By increasing the overconsolidation, the model predicts a final stiffness consistently higher than that obtained in the normally consolidated case, whereas the calculated damping ratio remains practically the same.

ii. The initial soil structure induces higher small-strain stiffness but its subsequent damage under cyclic loading leads to a higher rate of stiffness degradation in the medium to large strain range with respect to the unstructured case. Destructuration, on the contrary,

20

1   negligibly affects the behaviour in terms of hysteretic dissipation.

2   iii.   Overconsolidation and soil structure represent two distinct aspects of clay behaviour,

3   having opposite effects on G/G_0-γ, D-γ and $\Delta u/p_0$-γ curves.

4   iv.   The number of straining cycles is a fundamental parameter controlling the undrained

5   cyclic behaviour of clays. A number sufficient to reach a steady-state condition should be

6   adopted in numerical tests.

7   v.   The appropriate selection of the material parameters can lead to a realistic prediction of

8   hysteretic dissipation, although the model might over-predicts the damping ratio at large

9   strains.

10 A general good agreement between the main results of the numerical investigation and

11 experimental data on natural, reconstituted and compacted clays has been observed, thus

12 emphasizing the ability of the adopted model to capture crucial aspects of the cyclic behaviour of

13 clayey materials. Nevertheless, the work has highlighted some features of advanced modelling

14 which need further research. In particular, the evolution law of the plastic modulus during

15 unloading/reloading could be modified in future development of the *RMW* model to produce

16 smaller cycles and consequently improve the prediction of hysteretic dissipation in the large

17 strain range ($\gamma \geq 0.5\%$). It should also be noted that the cyclic simulations described in the paper

18 represent an oversimplification of real RC and TS experiments and cannot capture their intrinsic

19 dynamic nature. Full three-dimensional finite element simulations of these tests should be

20 performed in the future in order to improve the understanding of dynamic laboratory experiments

21 usually interpreted within the framework of visco-elasticity (e.g. Cundall [59], Pyke [60]). This

22 will assist in the development and validation of advanced constitutive models focusing on the

23 cyclic/dynamic behaviour of natural clays.

24

25

26

1 **Acknowledgements**

References

[1] Sangrey DA, Henkel DJ, Esrig MI. The effective stress response of a saturated clay soil to repeated loading. Can. Geotech. J. 1969;6(3):241-252.

[2] Castro G, Christian JT. Shear strength of soils and cyclic loading. J. Geotech. Eng. Div. ASCE 1976;102(GT9):887-894.

[3] Vucetic M, Dobry R. Effects of the soil plasticity on cyclic response. J. Geotech. Eng. ASCE 1991;117(1):89-107.

[4] Yasuhara K, Hirao K, Hyde AFL. Effects of cyclic loading on undrained strength and compressibility of clay. Soils and Foundations 1992;32(1):100-116.

[5] Matasović N, Vucetic M. Generalized cyclic-degradation-pore-pressure generation model for clays. J. Geotech. Eng. ASCE 1995;121(1):33-42.

[6] Lee C-J, Sheu S-F. The stiffness degradation and damping ratio evolution of Taipei Silty Clay under cyclic straining. Soil Dynam. Earth. Eng. 2007;27:730-740.

[7] Gu C, Wang J, Cai Y, Yang Z, Gao Y. Undrained cyclic triaxial behaviour of saturated clays under variable confining pressure. Soil Dynam. Earth. Eng. 2012;40:118-128.

[8] Burland JB. On the compressibility and shear strength of natural clays. Géotechnique 1990;40(3):329-378.

[9] Leroueil S, Vaughan PR. The general and congruent effects of structure in natural soils and weak rocks. Géotechnique 1990;40(3):467-488.

[10] Gens A, Nova R. Conceptual bases for a constitutive model for bonded soils and weak rocks. Proc. Int. Conf. on Hard Soils-Soft Rocks, Athens, Anagnostopoulos *et al*. Eds., Balkema, Rotterdam; 1993, p. 485-494.

[11] Burland JB, Rampello S, Georgiannou VN, Calabresi G. A laboratory study of the strength of four stiff clays. Géotechnique 1996;46:491-514.

[12] Cotecchia F, Chandler RJ. The influence of structure on the prefailure behaviour of a natural clay. Géotechnique 1997;47(3):523-544.

[13] Callisto L, Calabresi G. Mechanical behaviour of a natural soft clay. Géotechnique 1998;48(4):495-513.

[14] Callisto L, Rampello S. An interpretation of structural degradation for three natural clays. Can. Geotech. J. 2004;41:392-407.

[15] Amorosi A, Rampello S. An experimental investigation into the mechanical behaviour of a structured stiff clay. Géotechnique 2007;57(2):153-166.

[16] Lagioia R, Potts DM. The behaviour of shallow foundations on structured soils. Rivista Italiana di Geotecnica 1999;4:52-64.

[17] Nova R, Parma M, Castellanza R. Settlements of shallow foundations on soft rocks. Rivista Italiana di Geotecnica 2008;2:10-22.

[18] Karstunen M, Krenn H, Wheeler SJ, Koskinen M, Zentar R. The effect of anisotropy and destructuration on the behaviour of Murro test embankment. Int. J. Geomech. ASCE 2005;5(2):87-97.

[19] Panayides S, Rouainia M, Muir Wood D. Influence of degradation of structure on the behaviour of a full-scale embankment. Can. Geotech. J. 2012;49:344-356.

[20] Gonzáles NA, Rouainia M, Arroyo M, Gens A. Analysis of tunnel excavation in London Clay incorporating soil structure. Géotechnique 2012;62(12):1095-1109.

[21] Elia G, Rouainia M. Performance evaluation of a shallow foundation built on structured clays under seismic loading. Bulletin of Earthquake Engineering 2014;12(4):1537-1561.

[22] Rampello S, Silvestri F, Viggiani GMB. The dependence of small strain stiffness on stress state and history for fine grained soils: the example of Vallericca clay. Proc. 1st Int. Symp. on Pre-Failure Deformation of Geomaterials, Sapporo, Shibuya et al. Eds., Balkema, Rotterdam; 1994, Vol. 1, p. 273-278.

[23] Rampello S, Silvestri F, Viggiani GMB. The dependence of G_0 on stress state and history. Proc. 1st Int. Symp. on Pre-Failure Deformation of Geomaterials, Sapporo, Shibuya et al. Eds., Balkema, Rotterdam; 1995, Vol. 2, p. 1155-1160.

[24] Viggiani GMB, Atkinson JH. Stiffness of fine-grained soil at very small strains. Géotechnique 1995;45(2):249-265.

[25] Rampello S, Viggiani GMB. Pre-failure deformation characteristics of geomaterials. Proc. 2nd Int. Symp. on Pre-Failure Deformation of Geomaterials, Turin, Jamiolkowski et al. Eds., Balkema, Rotterdam; 2001, p. 1279-1289.

[26] Cafaro F, Cotecchia F. Structure degradation and changes in the mechanical behaviour of a stiff clay due to weathering. Géotechnique 2001;51(5):441-453.

[27] d'Onofrio A, Santucci de Magistris F, Olivares L. Influence of soil structure on the behaviour of two natural stiff clays in the pre-failure range. Proc. 2nd Int. Symp. on Hard Soils-Soft Rocks, Naples, Evangelista & Picarelli Eds., Balkema, Rotterdam; 1998, p. 497-505.

[28] d'Onofrio A, Vinale F, Silvestri F. Effects of micro-structure on the stress-strain behavior of two natural clays. Proc. 2nd Int. Symp. on Pre-Failure Deformation of Geomaterials, Turin, Jamiolkowski et al. Eds., Balkema, Rotterdam; 2001, p. 257-264.

[29] Rampello S, Silvestri F. The stress-strain behaviour of natural and reconstituted samples of two overconsolidated clays. Proc. Int. Conf. on Hard Soils-Soft Rocks, Athens, Anagnostopoulos et al. Eds., Balkema, Rotterdam; 1993, p. 769-778.

[30] Allman MA, Atkinson JH. Mechanical properties of reconstituted Bothkennar soil. Géotechnique 1992;42(2):289-301.

[31] Atkinson JH, Allman MA, Böese RJ. Influence of laboratory sample preparation procedures on the strength and stiffness of intact Bothkennar soil recovered using the Laval sampler. Géotechnique 1992;42(2):349-354.

[32] Ramberg W, Osgood WR. Description of stress-strain curves by three parameters. Technical Note No. 902, National Advisory Committee for Aeronautics, Washington DC; 1943.

[33] Iwan WD. On a class of models for the yielding behavior of continuous and composite systems. J. Appl. Mech. 1967;34:612-617.

[34] Duncan JM, Chang C-Y. Nonlinear analysis of stress and strain in soils. J. Soil Mech. Found. Div. ASCE 1970;96(SM5):1629-1653.

[35] Masing G. Eignespannungen und verfestigung beim messing. In: Second International Congress on Applied Mechanics, Zurich, Switzerland; 1926, p. 332-335.

[36] Pyke RM. Nonlinear soil models for irregular cyclic loadings. J. Geotech. Eng. Div. ASCE 1979;105(GT6):715-726.

[37] Puzrin AM, Shiran A. Effects of the constitutive relationship on seismic response of soils. Part I. Constitutive modeling of cyclic behavior of soils. Soil Dynam. Earth. Eng. 2000;19:305-318.

[38] Darendeli MB. Development of a new family of normalized modulus reduction and material damping curves. Ph.D. Thesis, University of Texas at Austin, USA; 2001.

[39] Phillips C, Hashash YMA. Damping formulation for nonlinear 1D site response analyses. Soil Dynam. Earth. Eng. 2009;29:1143-1158.

[40] Mroz Z, Norris VA, Zienkiewicz OC. An anisotropic hardening model for soils and its application to cyclic loading. Int. J. Num. Anal. Meth. Geomech. 1978;2:203-221.

[41] Prevost JH. Plasticity theory for soil stress-strain behaviour. J. Eng. Mech. ASCE 1978;104(5):1177-1194.

[42] Dafalias YF, Herrmann LR. Bounding surface plasticity. II: Application to isotropic cohesive soils. J. Eng. Mech. ASCE 1986;112(12):1263-1291.

[43] Asaoka A, Nakano M, Noda T. Superloading yield surface concept for highly structured soil behavior. Soils and Foundations 2000;40(2):99-110.

[44] Rouainia M, Muir Wood D. A kinematic hardening constitutive model for natural clays with loss of structure. Géotechnique 2000;50(2):153-164.

[45] Kavvadas M, Amorosi A. A constitutive model for structured soils. Géotechnique 2000;50(3):263-273.

[46] Baudet BA, Stallebrass SE. A constitutive model for structured clays. Géotechnique 2004;54(4):269-278.

[47] Seidalinov G, Taiebat M. Bounding surface SANICLAY plasticity model for cyclic clay behavior. Int. J. Numer. Anal. Meth. Geomech. 2014;38:702-724.

[48] Chan AHC. User Manual for DIANA-SWANDYNE II. University of Birmingham, UK; 1995.

[49] Elia G, Rouainia M. Seismic performance of earth embankment using simple and advanced numerical approaches. J. Geotech. Geoenv. Eng. ASCE 2013;139(7):1115-1129.

[50] Trhlíková J, Mašín D, Boháč J. Small-strain behaviour of cemented soils. Géotechnique 2012;62(10):943-947.

[51] Elia G. Analisi FEM di problem al contorno in condizioni statiche e dinamiche con un modello costitutivo avanzato. Ph.D. Thesis, Technical University of Bari, Italy; 2004.

[52] Elia G, Amorosi A, Chan AHC, Kavvadas M. Fully coupled dynamic analysis of an earth dam. Géotechnique 2011;61(7):549-563.

[53] Seed HB, Wong RT, Idriss IM, Tokimatsu K. Moduli and damping factors for dynamic analyses of cohesionless soils. J. Geotech. Eng. ASCE 1986;112(11):1016-1032.

[54] Vucetic M. Normalised behavior of offshore clay under uniform cyclic loading. Can. Geotech. J. 1988;25(1):33-41.

[55] Roscoe KH, Burland JB. On the generalized stress-strain behaviour of ''wet'' clay. In: Engineering plasticity. Cambridge: Cambridge University Press; 1968, p. 535-609.

[56] Meng J, Rix GJ. Reduction of equipment-generated damping in resonant column measurements. Géotechnique 2003;53(5):503-512.

[57] Soralump S, Prasomsri J. Cyclic pore water pressure generation and stiffness degradation in compacted clays. J. Geotech. Geoenv. Engrg. ASCE 2016;142(1):04015060.

[58] Zergoun M, Vaid YP. Effective stress response of clay to undrained cyclic loading. Can. Geotech. J. 1994;31(5):714-727.

[59] Cundall P. FLAC Version 4.0, User's Guide. Itasca Consulting Group, Minneapolis, USA; 2000.

[60] Pyke RM. TESS: a computer program for nonlinear ground response analyses. In: TAGA Engineering Systems and Software, Lafayette, California; 2000.

Appendix I: Constitutive model formulation

Figure 13 shows the three characteristic surfaces of the *RMW* model in the $p : q$ plane. The mathematical formulation of the model in the general stress space is summarised in the following. Since the model describes the response of the soil skeleton, all stresses are effective stresses (the primes have been dropped for simplicity). The expression of the reference surface is:

$$f_r = \frac{3}{2M_\theta^2} s : s + \left(p - p_c\right)^2 - \left(p_c\right)^2 = 0 \tag{I1}$$

The bubble surface is written as:

$$f_b = \frac{3}{2M_\theta^2}\left(s - s_{\bar{\alpha}}\right):\left(s - s_{\bar{\alpha}}\right) + \left(p - p_{\bar{\alpha}}\right)^2 - \left(Rp_c\right)^2 = 0 \tag{I2}$$

The structure surface is given by:

$$F = \frac{3}{2M_\theta^2}\left[s - (r-1)\boldsymbol{\eta}_0 p_c\right]:\left[s - (r-1)\boldsymbol{\eta}_0 p_c\right] + \left(p - rp_c\right)^2 - \left(rp_c\right)^2 = 0 \tag{I3}$$

where p_c is the effective stress which defines the size of the reference surface, R is the size of the bubble, M_θ is a dimensionless scaling function for deviatoric variation of the critical state stress ratio, $\boldsymbol{\eta}_0$ a deviatoric tensor controlling the structure, r is the ratio of the sizes of the structure and the reference surfaces, p and s are the mean pressure and deviatoric stress tensor and the symbol ':' indicates a summation of products. The dots over symbols indicate an infinitesimal increment of the corresponding quantity, whereas bold-face symbols indicate tensors.

The scalar variable r, which is a monotonically decreasing function of both plastic volumetric and shear strain, represents the progressive degradation of the material as follows:

$$\dot{r} = -\frac{k}{\left(\lambda^* - \kappa^*\right)}(r-1)\dot{\varepsilon}_d \tag{I4}$$

where λ^* and κ^* are the slopes of normal compression and swelling lines in the $\ln v : \ln p$ compression plane (being v the soil specific volume) and k is a parameter which controls the structure degradation with strain. The rate of the destructuration strain $\dot{\varepsilon}_d$ is assumed to have the following form:

$$\dot{\varepsilon}_d = \left[\left(1-A^*\right)\left(\dot{\varepsilon}_v^p\right)^2 + A^*\left(\dot{\varepsilon}_q^p\right)^2\right]^{1/2} \tag{I5}$$

where A^* is a non-dimensional scaling parameter and $\dot{\varepsilon}_q^p$ and $\dot{\varepsilon}_v^p$ are the plastic shear and volumetric strain rate, respectively.

Volumetric hardening rule is adopted in the model, where the change in size of the reference surface, p_c, is controlled only by plastic volumetric strain rate, $\dot{\varepsilon}_v^p$, given by:

$$\frac{\dot{p}_c}{p_c} = \frac{\dot{\varepsilon}_v^p}{\lambda^* - \kappa^*} \tag{I6}$$

If a stress increment requires movement of the bubble relative to the structure surface, the following kinematic hardening is invoked:

$$\dot{\bar{\alpha}} = \dot{\hat{\alpha}} + \frac{\dot{p}_c}{p_c}(\bar{\alpha} - \hat{\alpha}) + \dot{\mu}(\boldsymbol{\sigma}_c - \boldsymbol{\sigma}) \tag{I7}$$

where $\bar{\alpha}$ and $\hat{\alpha} = p_c \left[r\boldsymbol{I} + (r-1)\boldsymbol{\eta}_0 \right]$ denote the locations of the centre of the bubble and structure surface respectively, $\boldsymbol{\sigma}_c$ is the conjugate stress and μ is a positive scalar of proportionality. It should be noted that the centre of the structure surface and the deviator of $\hat{\alpha}$ represents the anisotropy of the soil due to structure. The deviator of $\hat{\alpha}$ therefore degrades to zero as r degrades to unity.

The plastic modulus H is assumed to depend on the distance between the current stress and the conjugate stress and is given by:

$$H = H_c + \frac{Bp_c^3}{(\lambda^* - \kappa^*)R}\left(\frac{b}{b_{\max}}\right)^{\psi} \tag{I8}$$

where H_c is the plastic modulus at the conjugate stress, B and ψ are two additional material properties, $b = \bar{\boldsymbol{n}} : (\boldsymbol{\sigma}_c - \boldsymbol{\sigma})$ is the normalised distance between the bubble and the structure surface and $b_{\max} = 2(r/R - 1)\bar{\boldsymbol{n}} : (\boldsymbol{\sigma} - \bar{\alpha})$ is its maximum value.

Notation:

A, m, n	non-dimensional factors in Equation (1)
b	normalised distance between bubble and structure surface
$b_{\max}$	maximum value of b
c_u	undrained shear strength
D	damping ratio
F	structure yield surface
f_r	reference yield surface
f_b	bubble yield surface
G_0	small-strain shear modulus
$G_{\sec}$	secant shear modulus
H	plastic modulus
H_c	plastic modulus at conjugate stress
$\boldsymbol{I}$	second rank identity tensor
K	bulk modulus
l	non-dimensional factor relating G_0 to structure in Equation (1)
N	number of cycles
$\bar{\boldsymbol{n}}$	normalised stress gradient on the bubble
p, p_0	mean effective stress
p_c	stress variable controlling size of the surfaces
q	scalar deviator stress
R_0	isotropic overconsolidation ratio
r	parameter describing ratio of sizes of structure and reference surfaces
r_u	normalised cyclic pore pressure
$\mathbf{s}$	tensorial deviator stress
$u, \Delta u$	pore and excess pore pressure
v	specific volume
$\bar{\alpha}$	location of the centre of the bubble
$\hat{\alpha}$	location of the centre of the structure surface
γ, γ_c	cyclic shear strain
ε_a	axial strain
ε_v^p	plastic volumetric strain

ε_q^p plastic deviatoric strain

ε_d damage strain

μ positive scalar of proportionality

$\boldsymbol{\sigma}$ effective stress tensor

$\boldsymbol{\sigma}_c$ conjugate stress

τ_c^*, τ_h^* normalised cyclic shear stress

ε_q^p plastic deviatoric strain

ε_d damage strain

Table 1 Model parameters and state variables – Set 1

Parameter/ state variable	Physical contribution/meaning	Set 1
λ^*	Slope of normal compression line in $\ln v : \ln p$ compression plane	0.11
κ^*	Slope of swelling line in $\ln v : \ln p$ compression plane	0.023
M_θ	Critical state stress ratio	1.20
R	Ratio of size of bubble and reference surface	0.10
B	Stiffness interpolation parameter	1.0
ψ	Stiffness interpolation exponent	1.5
A^*	Parameter controlling relative proportion of distorsional and volumetric destructuration	0.5
k	Parameter controlling rate of loss of structure with damage strain	1.0
ν	Poisson's ratio	0.25
p_0 (kPa)	Initial mean effective stress	varied
p_c (kPa)	Size of the reference surface	225
r_0	Initial degree of structure	varied
$\boldsymbol{\eta}_0$	Deviatoric tensor describing anisotropy of initial structure	**0**

Table 2 Model parameters – Sets 2, 3 and 4

	Set 2	Set 3	Set 4
λ^*	0.11	0.14	0.085
κ^*	0.023	0.012	0.012
M_θ	1.40	0.60	1.28
R	0.07	0.05	0.12
B	0.11	0.14	1.0
ψ	0.8	0.6	2.5
A^*	0.5	0.5	0.6
k	0.5	2.0	0.1
ν	0.25	0.25	0.25

Table 3 Model state variables – Set 2, 3 and 4

	Set 2	Set 3 NC	Set 3 OC	Set 4
p_0 (kPa)	100	1162	353	200
p_c (kPa)	67	447	544	35
r_0	3.0	1.3	1.3	3.0
$\boldsymbol{\eta_0}$	**0**	**0**	**0**	**0**
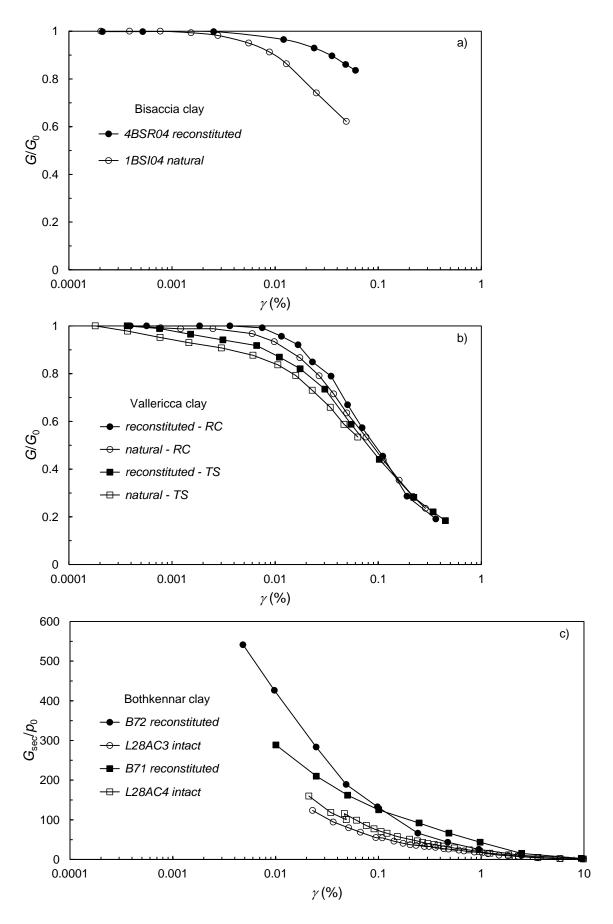
Fig. 1. Variation of normalised shear modulus with shear strain: (a) Bisaccia clay [27, 28]; (b) Vallericca clay [29]; (c) Bothkennar clay [30, 31].
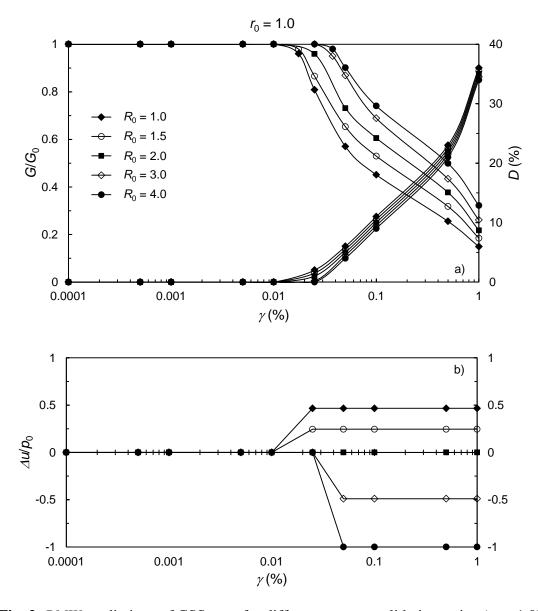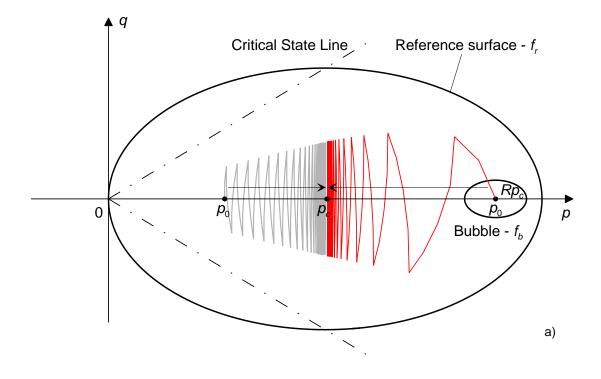
Fig. 2. *RMW* predictions of CSS tests for different overconsolidation ratios ($r_0 = 1.0$).
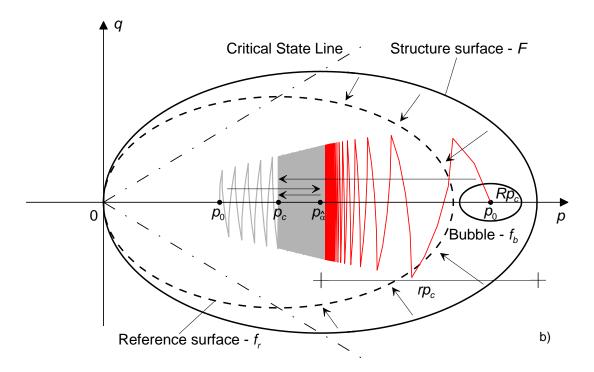
Fig. 3. *RMW* predictions of undrained triaxial tests on slightly and highly overconsolidated samples: (a) case with no structure; (b) case with structure.
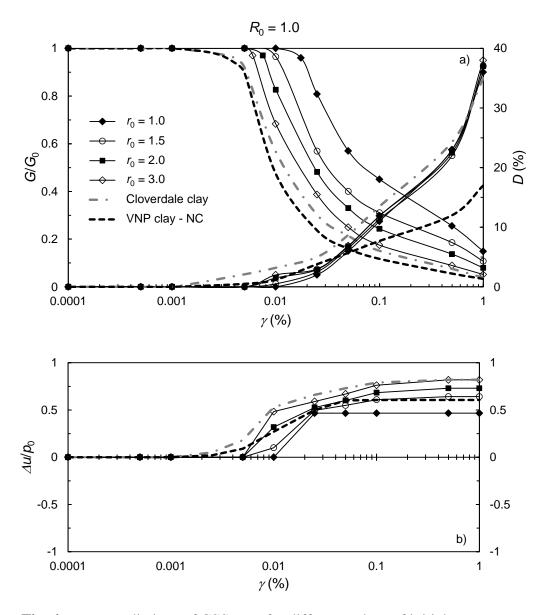
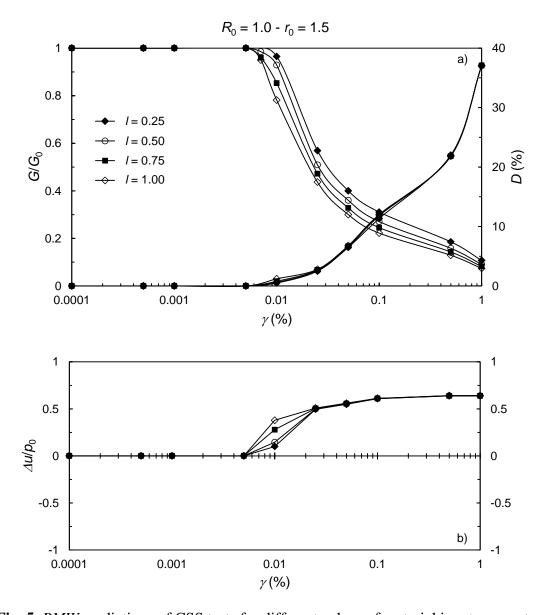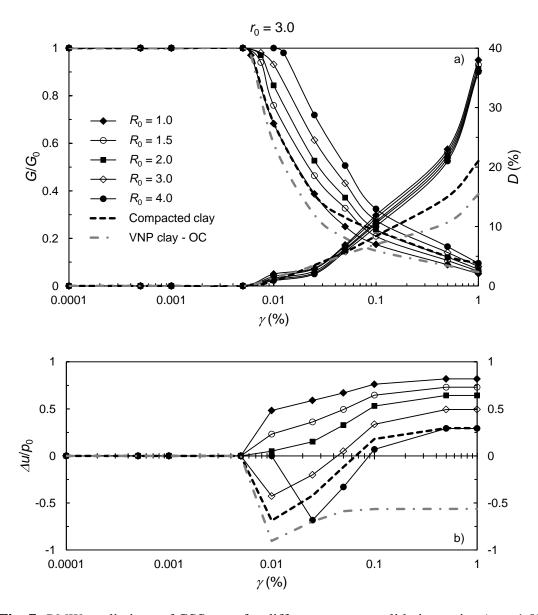**Fig. 4.** *RMW* predictions of CSS tests for different values of initial structure r_0.

Fig. 5. *RMW* predictions of CSS tests for different values of material input parameter *l*.
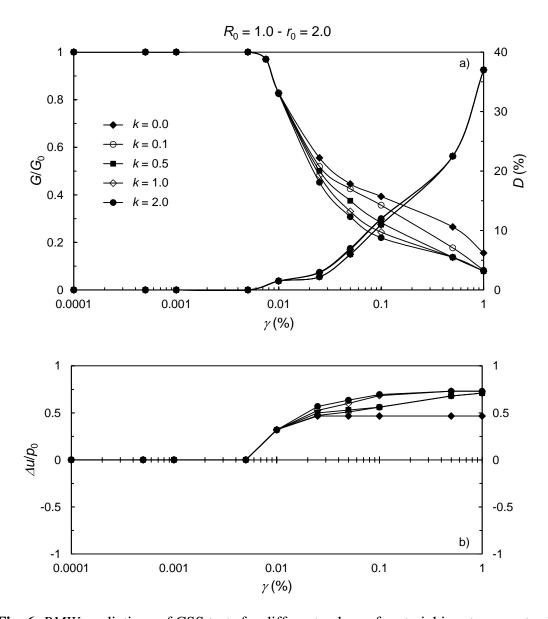
Fig. 6. *RMW* predictions of CSS tests for different values of material input parameter *k*.

Fig. 7. *RMW* predictions of CSS tests for different overconsolidation ratios ($r_0 \neq 1.0$).
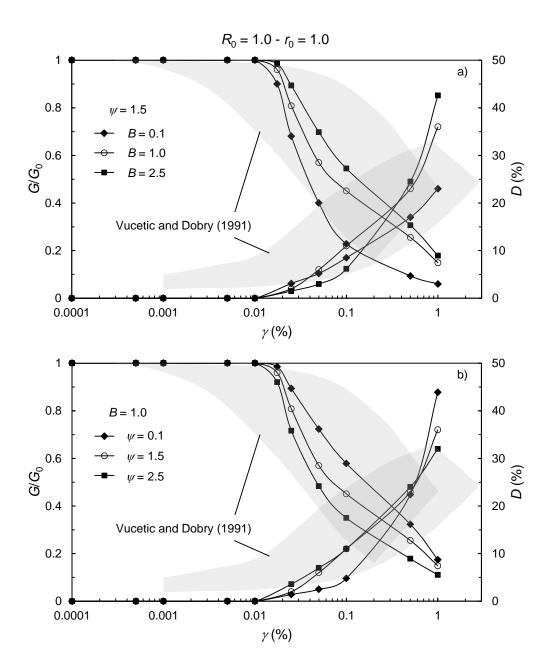
Fig. 8. *RMW* predictions of CSS tests for different values of material input parameters *B* and ψ.
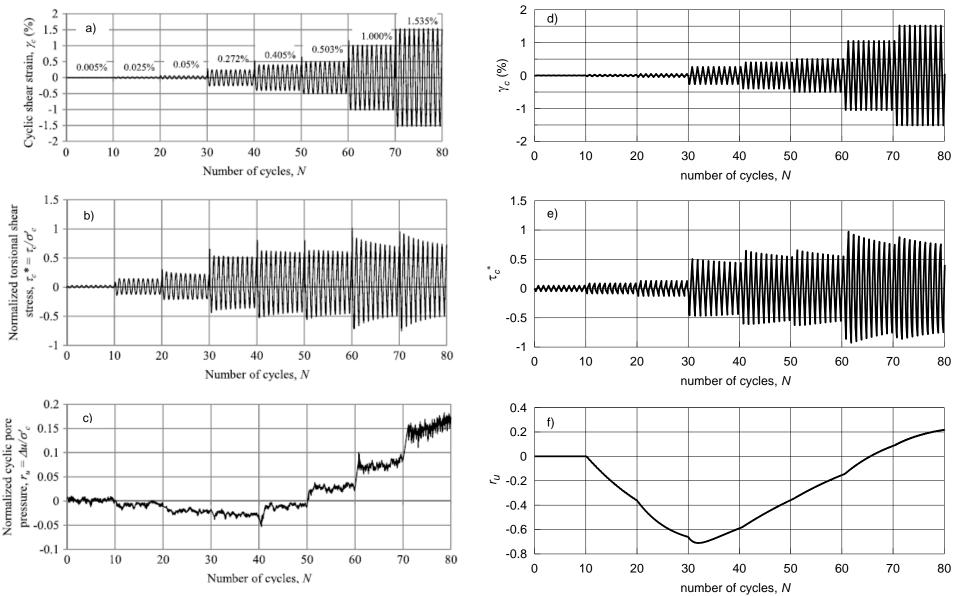
Fig. 9. Development of cyclic shear strain, normalised cyclic shear stress and pore water pressure with the number of cycles: (a-c) sample experimental data from [57]; (d-f) *RMW* predictions.
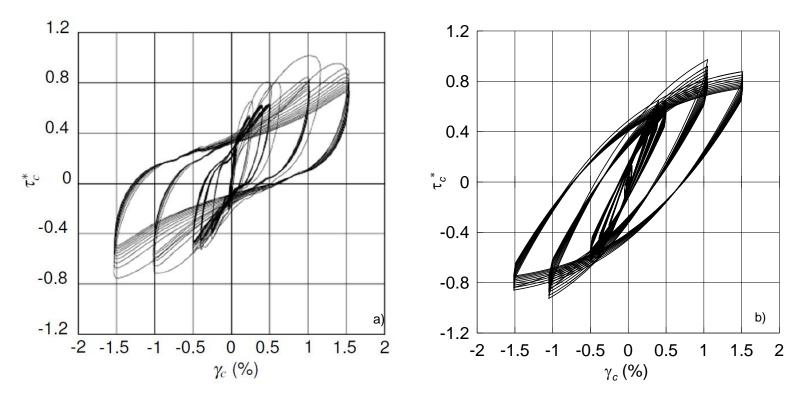
Fig. 10. Stress-strain hysteretic loops: (a) sample experimental data from [57]; (b) *RMW* predictions.
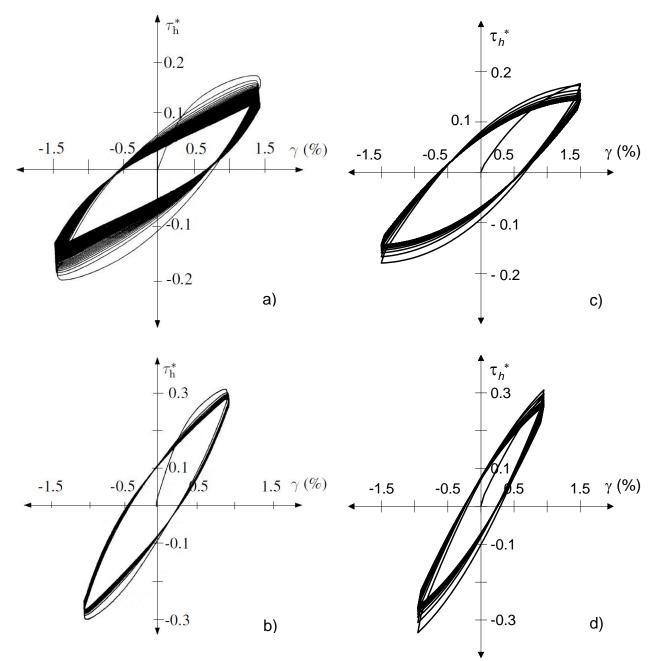
Fig. 11. Stress-strain hysteretic loops: (a-b) sample experimental data from [54]; (c-d) *RMW* predictions.
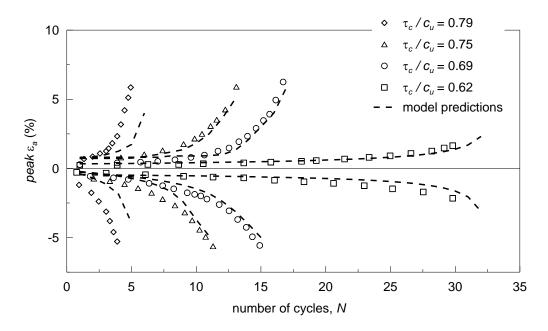
Fig. 12. Development of the axial strain ε_a at peaks of cyclic stress with the number of cycles: sample experimental data from [58] and *RMW* predictions.
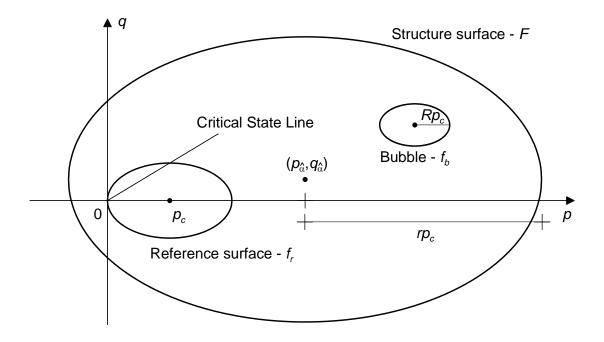
Fig. 13. *RMW* characteristic surfaces in the *p* : *q* plane.